Molecular Dynamics Simulations of Ligand-Induced Flap Closing in HIV-1 Protease Approach X-ray Resolution: Establishing the Role of Bound Water in the Flap Closing Mechanism†

Gurpreet Singh and Sanjib Senapati*

Department of Biotechnology, Indian Institute of Technology, Madras, Chennai 600036, India

Received April 16, 2008; Revised Manuscript Received August 18, 2008

ABSTRACT: The necessity of understanding the detailed mechanism of flap dynamics in designing HIV-1 protease inhibitors is immense. Crystal structures have provided us with a static overview of various conformations of the enzyme, but the existence of strong interplay among various conformations came to the fore only after dynamics studies. Here we elucidate the mechanistic aspects of HIV-1 protease flap closing upon binding inhibitors using all-atom molecular dynamics simulations. The unrestrained simulations reproduced not only the correct inhibitor-bound protease closed structures but also the structural water molecule which is seen in all protease−ligand X-ray structures. The study demonstrates that the structural water plays a critical role in flap closing dynamics by destabilizing the hydrophobic clusters and subsequently by mediating the flap−ligand interactions. Our results corroborate well with prior simulation and experimental findings and, at the same time, provide a molecular level description of the HIV-1 protease flap closing mechanism which can be crucial in the understanding of drug−receptor interactions.

The human immunodeficiency virus type 1 protease (HIV-1 protease) is one of the major targets for anti-AIDS therapy (*1*). The enzyme is a C_2-symmetric homodimer which is grouped under the family of aspartyl proteases (*2, 3*). Each monomer, containing 99 amino acid residues, has one α helix and two antiparallel β sheets in the secondary structure. The conserved catalytic triad is composed of Asp25-Thr26-Gly27 from each monomer with the Asp dyad constituting the active site base. The enzyme active site is gated by two extended β hairpin loops (residues 46−56), also known as flaps (*3*−*5*). The flaps contain three characteristic regions: the first region constituted by Met46-Phe53-Lys55 has the side chains extended outward toward solvent, the second region made up of Ile47-Ile54-Ile56 has the hydrophobic chain extended inward, and the third glycine-rich region is composed of Gly48-Gly49-Gly51-Gly52. The glycine-rich region in combination with Ile50 forms the highly flexible flap tip at the head of the flaps. That the flap flexibility is essential for efficient catalytic and activation processes in HIV-1 protease is now well documented (*6*−*10*), and this has led the researchers to target the flap movement in modulating the protease function (*11, 12*).

Recent experimental (*8, 9, 13*−*15*) and computational studies (*16*−*20*) have demonstrated that the flaps of the free enzyme can assume a variety of conformations. They can attain fully open, semiopen, and closed conformations. The NMR data suggest that these different conformations stay in equilibrium, with the semiopen form being the dominant one in unliganded protease (*8, 9*). The transition from the semiopen to open state is a slow process, which takes place in the time scale of nano- to microseconds (*8, 9*). Molecular dynamics (MD) simulation results support this proposition and demonstrated that the flaps of the native protease sample a large conformational space covering all three states (*19, 20*). A set of X-ray structures of free protease has been solved in recent years, and the existence of all three, open (*13*), semiopen (*14*), and closed (*15*), flap conformations were confirmed. In contrast, the closed conformation is seen in all ligand-bound (nonmutated) protease crystal structures (*21*−*25*). The study of mechanism of flap opening for ligand entry (or product release) and flap closing for ligand binding (or substrate hydrolysis) has therefore received tremendous attention in recent years. Note that the catalytic cycle of proteases involves three transformations (*26, 27*): (i) opening of the flaps to take up the substrate, (ii) closing of the flaps for proper placing and subsequent hydrolysis of the substrate, and (iii) reopening of the flaps to release the product. Although a few theoretical and computational reports are available on the flap opening mechanism (*16*−*18*), the study of the mechanism of flap closing in HIV-1 protease has been limited (*27, 28*).

A model of the flap closing mechanism in retroviral aspartic proteases was proposed only very recently by Toth and Borics (*27*). An implicit solvent simulation was carried out on the complex consisting of a peptide placed in the active site of HIV-1 protease with an open-flap conformation. The substrate was shown to induce the flap closing that leads to a closed-like structure of the protease−substrate complex. However, a relatively faster molecular movement due to the low-viscous solvent model did not allow the flaps to reach to the state as observed in X-ray structures. Hornak et al. (*28*) also have recently reported the closing of the flaps of

† This work was financially supported by the Department of Science and Technology (DST), Government of India.

* Address correspondence to this author. Tel: +91-44-2257-4122. Fax: +91-44-2257-4102. E-mail: sanjibs@iitm.ac.in.

10.1021/bi8006725 CCC: $40.75
Published on Web 09/12/2008

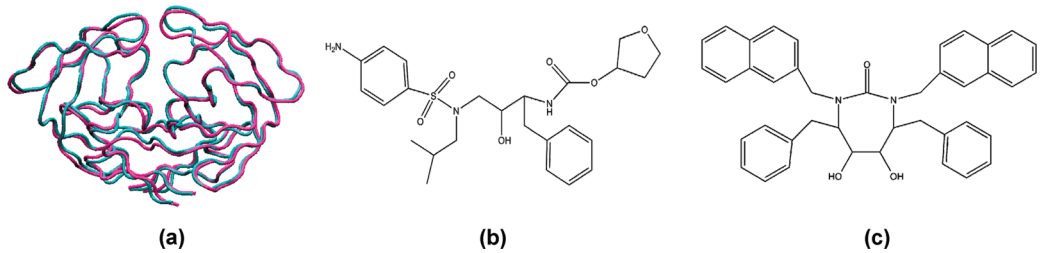

FIGURE 1: The starting open-flap conformations of HIV-1 protease are shown in (a): cyan, X-ray structure; magenta, MD-generated structure. Chemical structures of the inhibitors, amprenavir and XK263, which were docked into these enzyme structures are shown in (b) and (c).

HIV-1 protease induced by a cyclic urea inhibitor, manually placed into the binding site of the enzyme. Although their simulation in low-viscosity implicit water facilitates the flap closing on an affordable time, a quantitative comparison of time scales and the structural role of water during dynamic binding events could not be obtained. A good agreement in this study with X-ray structure was presumably due to the cyclic urea carbonyl oxygen which could mediate the flap tip−inhibitor interactions. Note that the resemblance of the carbonyl oxygen in cyclic urea-based inhibitors with a conserved interior water molecule in other ligand-bound HIV-1 protease complexes was validated by Torchia and co-workers (*29, 30*) from their NMR experiments. All of these results thus imply that the water plays a crucial role during protease flap conformational changes. An explicit treatment of solvent medium was therefore necessary to elucidate the mechanistic aspects of HIV-1 protease flap closing.

In this work, we describe the flap closing mechanism in HIV-1 protease by carrying out unrestrained, all-atom MD simulations of protease−inhibitor complexes in explicit solvent. The simulations were started by docking the inhibitors into the binding site cavities of open structures of HIV-1 protease. Inhibitors of two different kinds were considered in the study. An explicit three-site TIP3P water model was used as the surrounding medium. For comparison, a set of simulations in the implicit water model was also carried out. Our explicit solvent simulations reproduced not only the correct inhibitor-bound protease closed structures but also the structural water molecule which is seen in all ligand−protease X-ray structures to mediate the flap−inhibitor interactions. The simulated structures from implicit solvent simulations, on the other hand, were found to deviate significantly from the X-ray structures. A significant role of water during flap closing dynamics was also implicated from the study. Finally, a comparison of the dynamics of flap closing due to the binding of inhibitors of various natures was obtained which shows potential to support more efficient inhibitor design.

MATERIALS AND METHODS

We have chosen a recently crystallized apo, wild-type HIV-1 protease (*13*) with open-flap conformation as the starting structure for the enzyme (PDB ID 2PC0). Note that although the semiopen conformation is prevalent in unbound protease, it does not permit the ligand to access the active site. The flaps have to attain the open conformation to allow the ligand to get in and bind loosely to the active site (*8, 27, 28*). The stability of this starting structure was tested by carrying out 10 ns explicit solvent simulation, during which the protease is found to sample both the semiopen- and open-flap states. The inhibitors were docked into the binding site cavities of two of these open structures: (i) starting X-ray structure, open-A; (ii) revisited open structure during simulation, open-B. Ribbon representation of these structures is displayed in Figure 1. Inhibitors of two different natures were placed independently into these open structures, and the obtained inhibitor−protease complexes were subsequently simulated to explore the flap closing mechanism. Following the general perception that the ligand first binds loosely to the open structure (*10, 27, 28*), we placed the inhibitors roughly into the binding site with an initial inhibitor root mean square deviation (RMSD) ranging between 2 and 5 Å. The inhibitors we chose were a FDA (U.S. Food and Drug Administration) approved antiretroviral drug, amprenavir (*21*), and a cyclic urea-based protease inhibitor, XK263 (*24*). The rationale behind choosing XK263 was to compare the potency of the cyclic urea carbonyl oxygen in stabilizing the flaps with that of the conserved water found in most of the other inhibitor-bound closed crystal structures of the enzyme. The structures of the inhibitors were extracted from the complexes with PDB ID 1HPV and 1HVR, respectively. The chemical structures of these inhibitors are also shown in Figure 1.

Two primary sets of MD simulations of inhibitor−protease complexes were performed in this work. The first set of simulations was conducted in explicit water while a continuum solvent model was used in the second set. In each set, independent simulations of amprenavir−open-A protease, amprenavir−open-B protease, XK263−open-A protease, and XK263−open-B protease were carried out. For comparison, three additional simulations were performed in explicit water. In one of these, we simulated another amprenavir-HIV-1 PR complex structure where a representation of amprenavir was generated by a build-up approach (*31*) using the molecular builder software InsightII (*32*). The initial RMSD of this model amprenavir, with respect to the structure in 1HPV, was about 5 Å. Thus we simulated a total of 11 inhibitor−protease complexes in this study. A complete list of the systems that were investigated in this work is included in Table 1. In system 6 and system 7, the closed X-ray structures of amprenavir−protease (PDB ID 1HPV) and XK263−protease (PDB ID 1HVR) were simulated to compare the results from systems 1−5.

The three-site TIP3P model (*33*) for explicit water and the generalized Born model (*34*) for implicit water were chosen to describe the solvent environment. A set of partial atomic charges of the inhibitors was obtained via quantum electronic structure calculations. Using the Gaussian 03 program (*35*) with the 6-31G* basis set, we performed a

Table 1: List of Systems Investigated in This Study[a]

system	water model	starting conformation of HIV-1 PR	inhibitor
1a, 1b	explicit	open	amprenavir
2a, 2b	explicit	open	XK263
3a, 3b	implicit	open	amprenavir
4a, 4b	implicit	open	XK263
5	explicit	open	model amprenavir
6	explicit	closed	amprenavir
7	explicit	closed	XK263

[a] Systems *X*a and *X*b differ in their initial structure of the enzyme (*X* = 1, 2, 3, 4). While the simulations of *X*a were started from the protease X-ray structure, the simulations of *X*b were started from the MD-generated open structure.

Hartree−Fock geometry optimization procedure. The atom-centered RESP charges were determined via fits to the electrostatic potentials obtained from the calculated wave functions. Following the NMR reports on the protonation state of cyclic urea-bound HIV-1 proteases (*36*), we have protonated both of the catalytic Asp side chains in XK263-bound complexes. On the other hand, there is no specific experimental study on the protonation state of the catalytic aspartic acids in the amprenavir−HIV-1 PR complex. Based upon the available NMR data of a similar inhibitor−protease complex, KNI272−HIV-1 PR (*37*), we have treated Asp25 as protonated at OD2 and Asp25′ as deprotonated in all amprenavir-bound complexes.

All simulations were performed using the Amber 9.0 software package (*38*). For all of the PDB structures, hydrogens for heavy atoms were added by Leap in the Amber package. Added hydrogens were energy minimized for 500 steps using the steepest decent algorithm. The missing interaction parameters in the inhibitors were generated using antechamber (*39*) tools in Amber. After relaxing the added atoms in gas phase, each structure was solvated in a cubic box of water of 90 Å in length. Five chloride ions were randomly placed in the solvent to neutralize the charge of the protein. A set of minimization and thermalization runs of the starting structures was performed to remove the initial bad contacts. The systems were then equilibrated by MD simulations for 500 ps in the NPT ensemble followed by another 250 ps run in the NVT ensemble. All minimization and MD steps were performed with the Amber force fields. The time step used was 2 fs. All the simulations were carried out for 10 ns (5 ns for systems 6 and 7), and the implicit solvent simulations were carried out for 6 ns. Simulations were performed on four processors of a SGI Altix 390 linux cluster.

A targeted molecular dynamics (TMD) simulation (*40, 41*) was also performed on the equilibrated structure of system 5, obtained from 5 ns standard MD simulation. TMD is a method to induce a conformational transition relatively quickly by applying a time-dependent, purely geometrical restraint. The TMD simulation was performed by introducing an additional constraint force in a normal MD simulation. It incorporates an energy restraint based on the mass-weighted root mean square (RMS) distance of a set of atoms in the current conformation with respect to a reference target conformation. The functional form of the RMS restraint energy can be written as

$$E_{\mathrm{RMS}} = 0.5 k_{\mathrm{TMD}} M [D_{\mathrm{RMS}}(X(t), X^{\mathrm{target}}) - d_{\mathrm{o}}]^2$$

where k_{TMD} is the force constant, M is the number of constrained atoms, D_{RMS} represents the relative RMS distance for a selected set of atoms between the instantaneous conformation $X(t)$ and the reference X^{target}, and d_{o} is an offset constant in angstroms. With the decreasing of d_{o} (RMSD offset) as a function of the simulation time, the conformational change is driven from the initial to the final targeted conformation. In this study, the conformational change is driven by applying RMSD restraints only to heavy atoms of amprenavir.

RESULTS AND DISCUSSION

The simulations of loosely bound inhibitor−protease complexes, systems 1−5, were started, and the subsequent time evolutions were followed. As the simulations progressed, the protease was found to undergo inhibitor-induced transitions which ultimately led to closed-flap conformations, as found in all ligand-bound protease X-ray structures. We noted that the inhibitor−open-B HIV-1 protease complexes (systems 1b, 2b, 3b, and 4b) follow the same trajectories as the inhibitor−open-A protease complexes (systems 1a, 2a, 3a, and 4a). The similar results from inhibitor−open-B HIV-1 protease simulations were therefore omitted in the rest of the paper. Figure 2 shows a comparison of the final conformations that the inhibitor-bound open-A HIV-1 protease attained during the unrestrained simulations with the corresponding closed X-ray structures. The enzyme structures from the simulations are colored red, and those from the Protein Data Bank are colored cyan. The figures were generated by a stereo superposition of the crystal structures of the closed complex and the average structures of the complex from simulations, according to C_α atoms of HIV-1 protease. The average structures from simulations were obtained by taking the mean of the atom positions at every 10 ps interval during last 1 ns run. The figures clearly show that the simulation-generated structures match very well with the X-ray structures, particularly in explicit water. The structures in the implicit solvent, on the other hand, deviate sharply from X-ray structures. The RMSD values of the simulation-generated structures of the whole protease relative to the closed X-ray structures are included in Table 2. Notably the inhibitor RMSDs also reduced to 1.2−2.0 Å from high initial values, indicating that a proper placing of the inhibitors takes place during the protease flap closing event.

We, however, note that the more mobile flap regions contribute significantly to these structural differences in protease. Consequently, we have compared the dynamics of the flaps in both explicit and implicit solvents. Figure 3 depicts the time evolution of the RMSD of C_α atoms of flap residues (between M46 and I56) relative to the closed crystal structures. The implicit solvent simulations again produce larger deviations irrespective of the nature of the inhibitor. In the case of the XK263−protease simulation, however, the deviation is less, and the flaps reach to a closed state (see Figure 2d). A comparison of the time evolution of the flap tip−tip distances also supports this phenomenon (see Supporting Information). This can be explained due to the cyclic urea carbonyl oxygen in XK263 which provides some extent of stability to the protease flaps by accepting hydrogen bonds from the NH groups of Ile50/Ile50′. The most important point

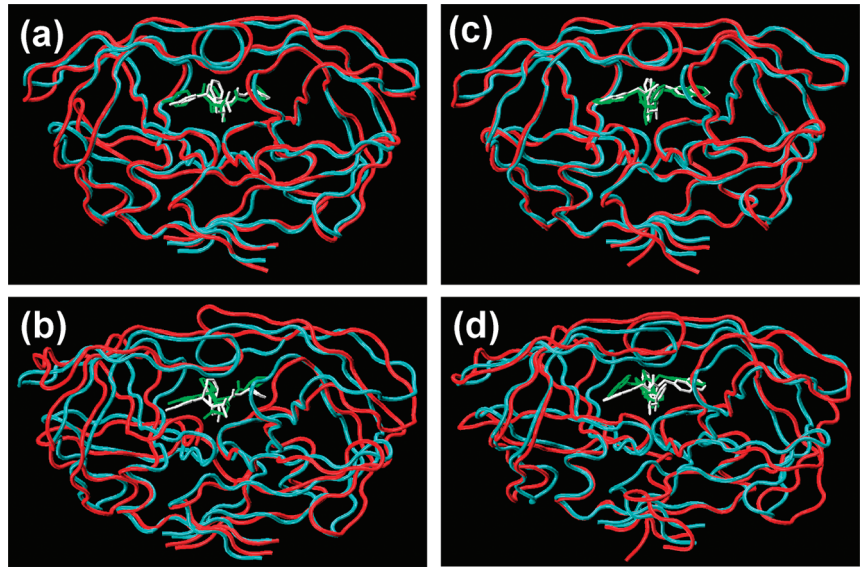

FIGURE 2: Comparison of the resultant structures of inhibitor-bound HIV-1 protease from MD simulations (red) with the X-ray structures (cyan). The resultant closed-flap conformations from amprenavir-bound protease simulations in explicit and implicit water are superimposed to 1HPV coordinates in (a) and (b). The respective conformations from XK263-bound protease simulations are superimposed to 1HVR in (c) and (d). The inhibitors are colored green in simulations and white in X-ray structures.

Table 2: Average RMSD of the Whole Protease Relative to the Closed X-ray Structures[a]

inhibitor	RMSD in explicit water	RMSD in implicit water
amprenavir	1.42 ± 0.05	2.84 ± 0.11
XK263	1.17 ± 0.07	3.00 ± 0.13

[a] Error ranges are determined by calculating RMSD for the last four 1 ns segments.

to note in this figure, however, is the gradual decrease of RMSD of both flaps, flap A and flap B, from about 8 to 1.3 Å in explicit water. Though this decay is a little faster in XK263−protease simulation, the mobility of flaps at subsequent times in this complex is also found to be more than in the amprenavir-bound complex. We will elaborate on this observation in the next sections. Figure 3 also points out that flap B in the amprenavir−protease complex goes to proper closing only at 6 ns, although flap A reached this state as early as 3 ns. By contrast, the large RMSD values in the implicit solvent amprenavir−protease simulation, particularly of flap B, indicate that it did not reach the crystal structure conformation (see Figure 2b). The insets in Figure 3 show a comparison of the results from these explicit simulations with the results from systems 6 and 7 to ensure that the flaps follow the right dynamics in postclosing sessions.

After finding that the protease flaps reach to the proper closed state in explicit water, we then explore the structural role of water that it played in stabilizing the flaps. Figure 4 shows a close-up view of the protease flaps along with the respective inhibitor. The structures were generated again by taking the mean of the atom positions at every 10 ps interval during the last 1 ns simulation run. In Figure 4a, also shown is a water molecule which appeared spontaneously at the flap−amprenavir interface during MD simulation. The analysis shows that this buried water was tetrahedrally coordinated and bridges the flaps of the protein to the inhibitor by accepting two hydrogen bonds (H-bonds) from the NH groups of Ile50/Ile50′ and donating two hydrogen bonds to CO groups of amprenavir. We will call this water "flap water". Interestingly, the existence of a conserved water molecule at this particular site was observed in all ligand-bound HIV-1 protease X-ray structures (*21*−*23*). Thus, our explicit solvent amprenavir−protease simulations reproduced not only the proper flap closure but also the conserved flap water, as seen in X-ray structures. However, a similar water molecule could not be located in the XK263−protease simulation; instead, the cyclic urea carbonyl oxygen embedded in XK263 was found to mediate the flap−inhibitor interactions as shown in Figure 4b. This result is also consistent with the NMR study which provided evidence for the displacement of the conserved water by a nonpeptide cyclic urea-based HIV protease inhibitor, DMP323 (*29, 30*).

The stability of the buried water and the time at which it appears at the flap−amprenavir interface were checked by further analyzing the trajectories over the simulation period. It was found that the water coordination shell started forming at around 2 ns, but the network became complete only at 6 ns. Once the tetrahedral coordination was reached, it remained intact for the rest of the 10 ns simulation. This subnanosecond residence time of the flap water again agrees favorably with NMR data (*30*). In the XK263−protease complex, however, we found that either one of the two flaps remains H-bonded to the carbonyl group of XK263. This is understandable, considering the rigidity that this CO group poses as being the part of a large inhibitor. The water molecule in the amprenavir−protease complex, on the other hand, can adjust its orientation at times to maintain a stable coordination shell. The stabilizing influence of this flap water was also analyzed from the interaction energy point of view, and the results are tabulated in Table 3. The results clearly indicate that the buried water in the amprenavir−protease complex induces much better stability to the protease flaps than the CO group in XK263. The differences in interaction energy values due to flap A and flap B also imply that the flaps in protease have differential flexibility. A comparison of the energy values with the results from quantum mechanical calculations of Duan et al. (*42*) shows a good agreement. The implicit solvent XK263−protease simulation also shows

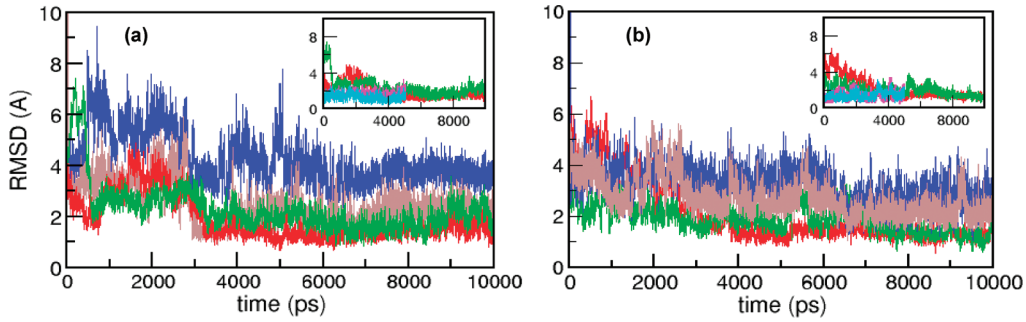

FIGURE 3: Time dependence of RMSD of the protease flaps in (a) amprenavir and (b) XK263 bound complexes. RMSD values were calculated by superposing the simulated structures with the closed-flap X-ray structures (1HPV and 1HVR, respectively) by fitting the C_α atoms of residues 1−45 and 57−99 of both monomers. Red and green are for flap A and flap B in explicit water simulations, brown and blue are for flap A and flap B in implicit solvent simulations. Cyan and pink in the insets are for flap A and flap B from the simulations of X-ray structures (a) 1HPV and (b) 1HVR in explicit water.

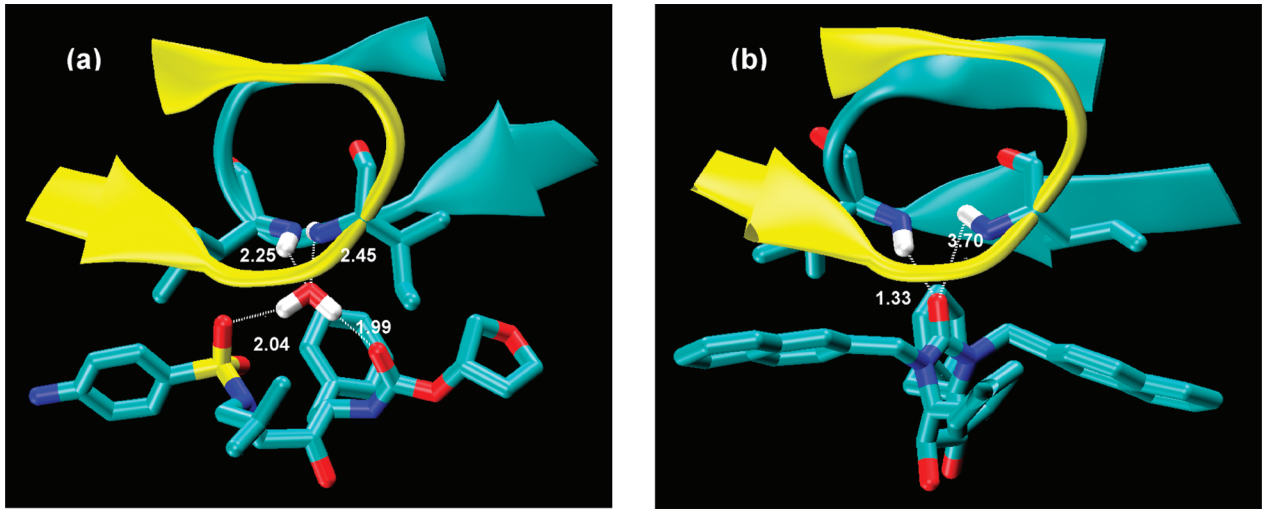

FIGURE 4: A close-up view of protease flaps along with bound (a) amprenavir and (b) XK263. In (a) also shown is a water molecule which appeared spontaneously at the flap−amprenavir interface during MD simulation. Flaps are shown in ribbon representation: yellow, flap A; cyan, flap B. Ile50 at the tip of each flap, inhibitors, and the water are drawn in stick representation. The color scheme in stick mode is as follows: cyan, C; blue, N; red, O; yellow, S; and white, water hydrogen. Other hydrogens are omitted for clarity. The dashed lines represent the possible modes of interactions (H-bonding), and the numbers represent the interatomic distances.

Table 3: Interaction Energies (kcal/mol) between Different Regions in the Inhibitor−Protease Complexes[a]

inhibitor	solvent	flap A−X	flap B−X	flap water−inhibitor
amprenavir	explicit	−2.64 ± 0.40	−1.72 ± 0.54	−8.81 ± 0.14
XK263	explicit	−2.34 ± 1.15	−0.91 ± 0.16	
XK263	implicit	−2.22 ± 1.00	−0.81 ± 0.06	

[a] Here X stands for flap water in the amprenavir-bound complex and CO group in the XK263-bound complexes. Error ranges are determined by calculating energies for the last four 1 ns segments.

a similar pattern in CO-mediated inhibitor−flap interactions. Nonetheless, it is worth mentioning that the subtle differences between explicit and implicit solvent simulation results arise from the influence of the surrounding water.

In Figure 5, we have produced a graphical representation of flap conformational transitions in inhibitor-bound HIV-1 protease. In an attempt to compare the extent of flap closing in various environments, results from system 1, system 3, and system 4 are presented. System 1 differs from system 3 in solvent type, and system 4 differs from the other two systems in inhibitor type. As shown, the flap water in explicit solvent simulation of the amprenavir−protease complex (system 1) appeared spontaneously and allowed the flaps to close down. In implicit solvent simulation of the same complex in system 3, however, the flaps display large fluctuations, and the complex was never stabilized in the closed state. Very interestingly, even in implicit solvent simulation the protease flaps reach to the closed conformation while bound to the cyclic urea carbonyl oxygen-based inhibitor, XK263 (system 4). Note that this carbonyl oxygen in XK263 resembles flap water, and the flap water was not found in explicit water XK263−protease simulation.

This implies that the flap water or cyclic urea carbonyl oxygen is directly involved in flap closing dynamics and in subsequent stabilization of the flaps in ligand-bound HIV-1 proteases. To recheck this finding, we have plotted the variation of distances of the flaps and flap water with respect to protease catalytic residues Asp25 and Asp25′ for system 1, and that is shown in Figure 6. As the flaps close over the active site or the flap water travels toward bound amprenavir, these distances diminish. A detailed analysis of the system structures (as exemplified in Figure 5) and related time scales (as in Figure 6) demonstrates the following mechanism of protease flap closing.

There exists a strong correlation between the internal motion of the protease active site cavity and the conformational exchange of flap tips. In the first 20 ps of simulations, the active site residues experience slight outward movement

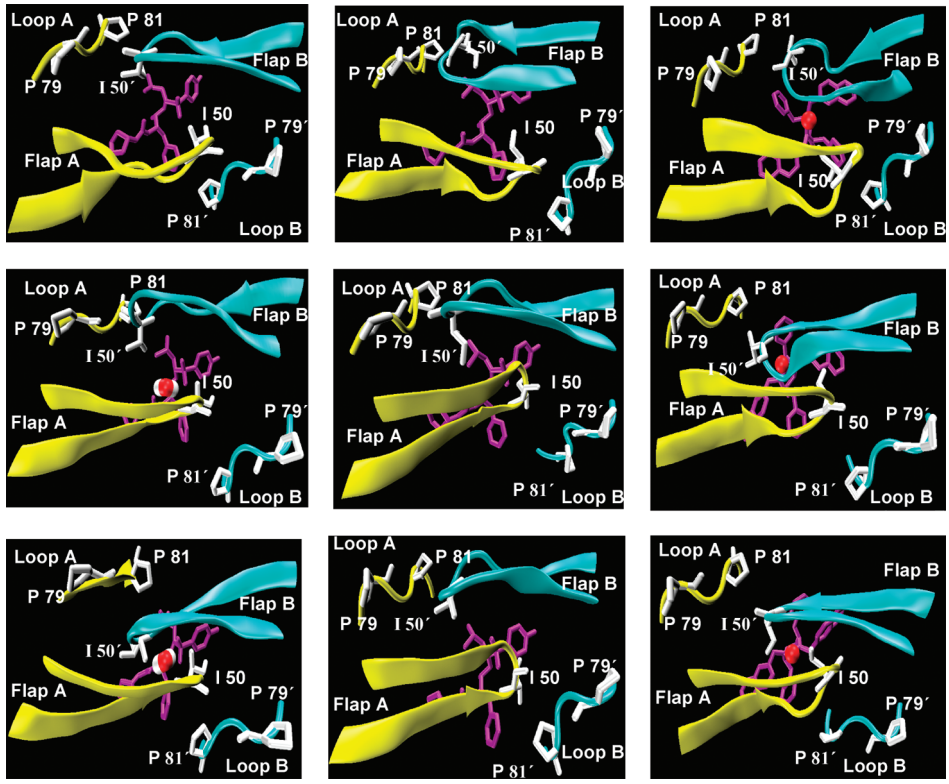

FIGURE 5: The mechanism of HIV-1 protease flap closing upon binding inhibitors. In a view from the top looking down toward the active site, only flap A, flap B, loop A, loop B, flap water, and the inhibitors are shown. The column on the left shows the snapshots from amprenavir-bound HIV-1 protease explicit solvent simulation, the column at the center shows the snapshots from amprenavir-bound HIV-1 protease implicit solvent simulation, and the column on the right shows the snapshots from XK263-bound HIV-1 protease implicit solvent simulation. The structures in each column are generated at 1, 3, and 6 ns (from top to bottom). Inhibitors are colored purple in all, but the cyclic urea carbonyl oxygen in XK263 is highlighted in red. Water is shown in red and white stick. At 1 ns of explicit solvent simulation when the flap water did not appear in the active site cavity, both flap A and flap B remained in hydrophobic clusters with loop B and loop A.

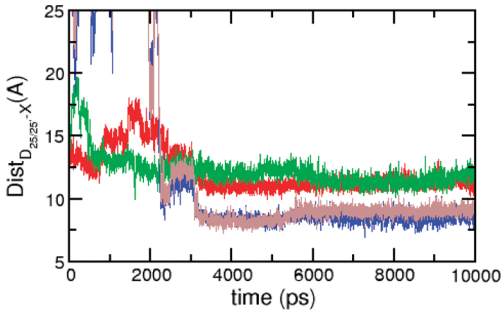

FIGURE 6: The variation of distances of flaps and flap water from protease catalytic residues Asp25 and Asp25′ for system 1. The color scheme is as follows: red, Asp25−flap A; green, Asp25′−flap B; blue, Asp25−water; gray, Asp25′−water.

on inhibitor binding, and that induces certain changes in the flap tip conformation. Flap A straightens up a little farther, and both of the flap tips move more toward the 80s loop of the opposite subunit to hide their hydrophobic chains from the surrounding water environment. This leads to the formation of hydrophobic clusters (*27*), mainly composed of the side chains of Ile50 on the tip, proline residues 79 and 81 in the loop, and the side chains of amprenavir (Figure 5). The rearrangement takes about 800 ps, and the formed cluster lasted for about 2700 ps in case of flap B. For flap A, however, the hydrophobic cluster was quite fluctuating and breaks at 2.3 ns when it makes contact with flap water. The flap water visits the protease active site cavity first at 2.2 ns but leaves immediately after finding no suitable environment (Figure 6). The water therefore goes back to bulk, forms a hydrogen bond with Ile50 of flap A, and then at 3 ns falls upon the active site along with flap A to close the cavity (Figures 5 and 6). The RMSD of flap A thus drops down to 1.3 Å at this time, but for flap B it still remains high. Closing of flap A causes some extent of instability inside the hydrophobic cluster of flap B, and that triggers the buried hydroxyl side chain of Thr80 to get solvent exposed. Maintaining the formed H-bond with flap A, the flap water flips around to find a connection with flap B. At around 6 ns when this water manages to make a contact with flap B, flap B closed over the active site to help the enzyme attain the proper closed state (Figures 5 and 6). These times of flap closing (3 ns for flap A and 6 ns for flap B) are very much consistent with Figure 3. The values also fall in the predicted time scale of picoseconds to microseconds from NMR experiments (*7*−*10*).

In the case of XK263-bound complexes, the carbonyl oxygen of docked XK263 becomes localized almost at the same position where the flap water in the amprenavir-bound protease structure gets stabilized. A comparison of two closed structures, after superposition, shows that flap water in system 1 is only 0.6 Å above the carbonyl oxygen in system 2. The presence of the carbonyl oxygen at this location from an earlier time, therefore, destabilizes the hydrophobic clusters more quickly than flap water in system 1 and thus induces a faster flap closing. However, a rigid nature of this carbonyl group could not make the flaps as inflexible as the flap water

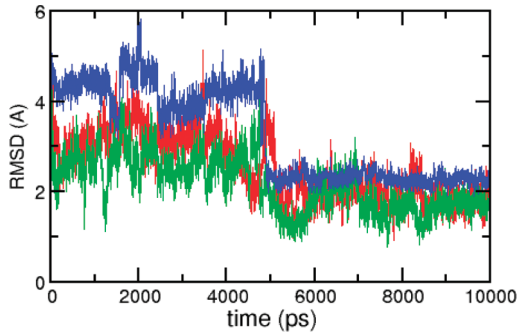

FIGURE 7: RMSD values of flap A (red), flap B (green), and model amprenavir (blue) during combined TMD and MD simulations in system 5. The sequence of simulations was 5 ns MD, 0.5 ns TMD, and 5 ns MD. The RMSD values are calculated as described in Figure 3a.

could do, which is evident from Table 3. Nevertheless, the carbonyl oxygen-mediated flap−XK263 interactions are strong enough to take the protease to a closed state. To strengthen our findings further, we ran a control simulation for the protease bound XK263 derivative in implicit solvent wherein the cyclic C═O of XK263 was replaced by CH_2. In contrast to XK263, a much larger flap RMSD was observed in this case (see Supporting Information). Thus a direct involvement of flap water or cyclic urea carbonyl oxygen in the flap closing mechanism of ligand-bound HIV-1 protease became evident from this study.

The coordinates of the docked inhibitors in systems 1−4 were obtained from Protein Data Bank. In system 5, we simulated an amprenavir-bound protease structure where the amprenavir coordinates were generated using the model building tool in InsightII (*32*). The initial RMSD of this model amprenavir, with respect to the X-ray structure 1HPV, was about 5 Å. An explicit solvent MD simulation carried out for 5 ns on this system shows larger fluctuations in the inhibitor structure than those observed in system 1. The results indicated that a conformational transition could take place in the protein−inhibitor structure over a longer simulation time. We therefore introduced TMD in this system to induce the conformational transition relatively quickly. The TMD simulation necessarily performs a best fit of the simulation structure of the inhibitor to the PDB structure (*40, 41*). The TMD simulation was performed with a force constant 2.0 kcal mol^{-1} $Å^{-2}$. At this value of the force constant, the inhibitor reaches almost the target structure in just 500 ps of simulation time. Subsequently, we find that the flap water spontaneously appeared at the right location, and both of the flaps closed over the active site. The RMSD of the flaps and the inhibitor drops down to 2.0 Å and remains so, even though TMD was taken off. To further check the stability of the transformed structure, we performed MD simulation on this structure for another 5 ns and found that the closed structure remained stable thereafter. These results are presented in Figure 7. The detailed analysis again shows a similar mechanism of flap closing involving the flap water. Thus the simulations of system 1 and system 5 imply that the starting configuration has little correlation with the long-time dynamics (*43*), and computer simulations have the ability to reproduce large-scale receptor conformational changes (*19, 28*). It is worth mentioning here that the other surrounding water molecules would also have a significant influence on protease dynamics. Nonetheless, the direct involvement of flap water in protease's closing mechanism readily emerges from this study.

SUMMARY AND CONCLUSIONS

To summarize, we have explored the functional aspects of bound water in HIV-1 protease flap closing dynamics by carrying out unrestrained all-atom molecular dynamics simulations. Inhibitors of two different natures were docked into the active site cavities of open-flap conformations of the enzyme, and the subsequent dynamics were followed in two different solvent models. The simulation of the amprenavir−protease structure in explicit water reproduced not only the correct closed state of the enzyme but also the structural water molecule seen in all protease−ligand X-ray structures. The simulated structure in implicit solvent, in contrast, deviates significantly. On the other hand, the cyclic urea carbonyl oxygen-based inhibitor, XK263, stabilizes the protease flaps both in explicit and in implicit solvent simulations. Analysis shows that the cyclic urea carbonyl oxygen in XK263 occupies exactly the same position where the structural water in explicit water amprenavir−protease simulation sits, indicating that the structural water plays a crucial role in stabilizing the flaps. More importantly, however, this water is found to be involved in the flap closing mechanism as well. The instability of flaps in implicit solvent amprenavir−protease simulation clearly indicates that the hydrophobic clustering is not a strong enough stimulus to induce protease flap closing. The structural water (or the cyclic urea carbonyl oxygen in XK263) rather perturbs the hydrophobic clusters, formed between each flap and the opposite loop, and directs the flaps to move toward the inhibitor such that a favorable flap water−inhibitor interaction can take place. Thus a direct involvement of the structural water in the protease's flap closing mechanism readily emerges from the study. Although the existence of bound water in ligand-bound proteases was known from experimental reports, its involvement in flap closing dynamics became evident, for the first time, from this computer simulation study. The study also brought to the notice that the solvent not only helps the protease in substrate hydrolysis but also helps in attaining the right geometry for hydrolytic reaction to occur. Finally, the differential flap flexibility and inhibitor−protease interaction energies in amprenavir and XK263-bound complexes tempted us to conclude that the inhibitors with two carbonyl functional groups would be more potent drug candidates than the ones with a single cyclic urea carbonyl group. As a matter of fact, all nine FDA-approved protease drugs contain two CO functional groups.

SUPPORTING INFORMATION AVAILABLE

Complete citation of refs *35* and *38*, the time evolution of the flap tip−tip distances, and the control simulation RMSDs. This material is available free of charge via the Internet at http://pubs.acs.org.

REFERENCES

1. Kohl, N. E., Emini, E. A., Schleif, W. A., Davis, L. J., Heimbach, J. C., Dixon, R. A., Scolnick, E. M., and Sigal, I. S. (1988) Active human immunodeficiency virus protease is required for viral infectivity. *Proc. Natl. Acad. Sci. U.S.A. 85*, 4686–4690.
2. Miller, M., Jaskolski, M., Rao, J. K. M., Leis, J., and Wlodawer, A. (1989) Crystal structure of a retroviral protease proves relationship to protease family. *Nature 337*, 576–579.
3. Lapato, R., Blundell, T., Hemmings, A., Overington, J., Wilderspin, A., Wood, S., Merson, J. R., Whittle, P. J., Danley, D. E.,

Geoghegan, K. F., Hawrylik, S. J., Lee, S. E., Scheld, K. G., and Hobart, P. M. (1989) X-Ray analysis of HIV-1 Proteinase at 2.7Å resolution confirms structural homology among retroviral enzymes. *Nature 342*, 299–302.
4. Wlodawer, A., Miller, M., Jaskolski, M., Sathyanaryana, B. K., Baldwin, E., Weber, I. T., Selk, L. M., Clawson, L., Schneider, J., and Kent, S. B. H. (1989) Conserved folding in retroviral proteases: Crystal structure of a synthetic HIV-1 protease. *Science 245*, 616–621.
5. Navia, M. A., Fitzgerald, P. M. D., McKeever, B. M., Leu, C. T., Heimbach, J. C., Herber, W. K., Sigal, I. S., Darke, P. L., and Springer, J. P. (1989) Three dimensional structure of aspartyl protease from human immunodeficiency virus HIV-1. *Nature 337*, 615–620.
6. Shao, W., Everitt, L., Manchester, M., Loeb, D. D., Hutchison, C. A., and Swanstrom, R. (1997) Sequence requirements of the HIV-1 protease flap region determined by saturation mutagenesis and kinetic analysis of flap mutants. *Proc. Natl. Acad. Sci. U.S.A. 94*, 2243–2248.
7. Nicholsan, L. K., Yamazaki, T., Torchia, D. A., Grzesiek, S., Bax, A., Stahl, S. J., Kaufman, J. D., Wingfield, P. T., Lam, P. V. S., Jadhav, P. K., Hodge, C. N., Domaille, P. J., and Chang, C. H. (1995) Flexibility and function in HIV-1 protease. *Nat. Struct. Biol. 2*, 274–280.
8. Ishima, R., Freedberg, D., Wang, Y. X., Louis, J. M., and Torchia, D. A. (1999) Flap opening and dimmer-interface flexibility in the free and inhibitor bound HIV protease, and their implications for function. *Structure 7*, 1047–1055.
9. Freedberg, D. I., Ishima, R., Jacob, J., Wang, Y. X., Kustanovich, I., Louis, J. M., and Torchia, D. A. (2002) Rapid structural fluctuations of HIV-1 Protease flaps in solution: Relationship to crystal structures and comparison with predictions of dynamic calculations. *Protein Sci. 11*, 221–232.
10. Katoh, E., Louis, D. A., Yamazaki, T., Gronenborn, A. M., Torchia, D. A., and Ishima, R. (2003) A solution NMR study of the binding kinetics and the internal dynamics of an HIV-1 protease-substrate complex. *Protein Sci. 12*, 1376–1385.
11. Perryman, A. L., Lin, J. H., and McCammon, J. A. (2006) Restrained molecular dynamics simulations of HIV-1 protease: The first step in validating a new target for drug design. *Biopolymers 82*, 272–284.
12. Hornok, V., and Simmerling, C. (2007) Targeting structural flexibility in HIV-1 protease inhibitor binding. *Drug Discov. Today 12*, 132–138.
13. Heaslet, H., Rosenfeld, R., Giffin, M., Lin, Y. C., Torbett, B. E., Elder, J. H., McRee, D. E., and Stout, C. D. (2007) Conformational flexibility in the flap domains of ligand-free HIV-1 protease. *Acta Crystallogr. D 63*, 866–875.
14. Spinelli, S., Lin, Q. Z., Alzari, P. M., Hirel, P. H., and Polzak, R. J. (1991) The three dimensional structure of aspartyl protease from HIV-1 isolate BRU. *Biochimie 73*, 1391–1396.
15. Pillai, B., Kannan, K. K., and Hosur, M. V. (2001) 1.9Å X-ray study shows closed flap conformation in crystals of tethered HIV-1 PR. *Proteins 43*, 57–64.
16. Collins, J. R., Burt, S. K., and Erickson, J. W. (1995) Flap opening in HIV-1 protease simulated by activated molecular dynamics. *Nat. Struct. Biol. 2*, 334–338.
17. Scott, W. R. P., and Schiffer, C. A. (2000) Curling of flaps tips in HIV-1 protease as a mechanism for substrate entry and tolerance of drug resistance. *Structure 8*, 1259–1265.
18. Toth, G., and Borics, A. (2006) Flap opening mechanism of HIV-1 protease. *J. Mol. Graphics Modell. 24*, 465–474.
19. Hornok, V., Okur, A., Rizzo, R. C., and Simmerling, C. (2006) HIV-1 protease flaps spontaneously open and reclose in molecular dynamics simulations. *Proc. Natl. Acad. Sci. U.S.A. 103*, 915–920.
20. Tozzini, V., Trylska, J., Chang, C. E., and McCammon, J. A. (2007) Flap opening dynamics in HIV-1 protease explored with coarse grained model. *J. Struct. Biol. 157*, 606–615.
21. Kim, E. E., Baker, C. T., Dwyer, M. D., Murcko, M. A., Rao, B. G., Tung, R. D., and Navia, M. A. (1995) Crystal structure of HIV-1 protease in complex with vx-478, a potent and orally bioavailable inhibitor of the enzyme. *J. Am. Chem. Soc. 117*, 1181–1182.
22. Clemente, J. C., Coman, R. M., Thiaville, M. M., Janka, L. K., Jeung, J. A., Nukoolkarn, S., Govindasamy, L., Agbandje-McKenna, M., McKenna, R., Leelamanit, W., Goodenow, M. M., and Dunn, B. M. (2006) Analysis of HIV-1 CRF_01 A/E protease inhibitor resistance: Structural determinants for maintaining sensitivity and developing resistance to atazanavir. *Biochemistry 45*, 5468–5477.
23. Reddy, G. S., Ali, A., Nalem, M. N., Anjum, S. G., Cao, H., Nathans, R. S., Schiffer, C. A., and Rana, T. M. (2007) Design and synthesis of HIV-1 protease inhibitors incorporating oxazolidinones as P2/P2′ ligands in pseudosymmetric dipeptide isosteres. *J. Med. Chem. 50*, 4316–4328.
24. Lam, P. Y., Jadhav, P. K., Eyermann, C. J., Hodge, C. N., Ru, Y., Bacheler, L. T., Meek, J. L., Otto, M. J., Rayner, M. M., Wong, Y. N., Chang, C. H., Weber, P. C., Jackson, D. A., Sharpe, T. R., and Ericksonviitanen, S. (1994) Rational design of potent, bioavailable, non-peptide cyclic urea as HIV protease inhibitors. *Science 263*, 380–384.
25. Lam, P. Y. (1996) Cyclic HIV protease inhibitors: Synthesis, conformational analysis, P2/P2′ structure activity relationship, and molecular recognition of cyclic ureas. *J. Med. Chem. 39*, 3514–3525.
26. Dunn, B. M. (2002) Structure and mechanism of pepsin-like family of aspartic peptidases. *Chem. Rev. 102*, 4431–4458.
27. Toth, G., and Borics, A. (2006) Closing of the flaps of HIV-1 protease induced by substrate binding: A model of flap closing mechanism in retroviral aspartic proteases. *Biochemistry 45*, 6606–6614.
28. Hornok, V., Okur, A., Rizzo, R. C., and Simmerling, C. (2006) HIV-1 protease flaps spontaneously close to the correct structure in simulations following manual placements of an inhibitor in the active site. *J. Am. Chem. Soc. 128*, 2812–2813.
29. Grzesiek, S., Bax, A., Nicholson, L. K., Yamazaki, T., Wingield, P., Stahl, S. J., Eyermann, C. J., Torchia, D. A., Hodge, C. N., Lam, P. V. S., Jadhav, P. K., and Chang, C. H. (1996) NMR evidence for the displacement of a conserved water molecule in HIV-1 protease by a non-peptide cyclic urea based inhibitor. *J. Am. Chem. Soc. 116*, 1581–1582.
30. Wang, Y. X., Freedberg, D. I., Grzesiek, S., Torchia, D. A., Wingfield, P. T., Kaufman, J. D., Stahl, S. J., Chang, C. H., and Hodge, C. N. (1996) Mapping hydration water molecules in HIV-1 protease/DMP323 complex in solution by NMR spectroscopy. *Biochemistry 35*, 12694–12704.
31. Wang, R., Gao, Y., and Lai, L. (2000) LigBuilder: A multipurpose program for structure based drug design. *J. Mol. Model. 6*, 498–516.
32. InsightII (1996) Accelrys, Inc., 9685 Scranton Road, San Diego, CA.
33. Jorgensen, W. L., Chandrasekhar, J., and Madura, J. D. (1983) Comparison of simple potential functions for simulating liquid water. *J. Chem. Phys. 79*, 926–935.
34. Onufriev, A., Bashford, D., and Case, D. A. (2000) Modification of generalized Born model suitable for macromolecules. *J. Phys. Chem. B 104*, 3712–3720.
35. Frisch, M. J., et al. (2004)Gaussian 03, Revision C.02, Gaussian Inc., Wallingford, CT.
36. Yamazaki, T., Nicholsan, L. K., Torchia, D. A., Wingfield, P., Stahl, S. J., Kaufman, J. D., Eyermann, C. J., Hodge, C. N., Lam, P. Y. S., Ru, Y., Jadhav, P. K., Chang, C. H., and Weber, P. C. (1994) NMR and X-ray evidence that the HIV protease catalytic aspartyl groups are protonated in the complex formed by protease and a non-peptide cyclic urea based inhibitor. *J. Am. Chem. Soc. 116*, 10791–10792.
37. Wang, Y. X., Freedberg, D. I., Yamazaki, T., Wingfield, P. T., Stahl, S. J., Kaufman, J. D., Kiso, Y., and Torchia, D. A. (1996) Solution NMR evidence that the HIV-1 protease catalytic aspartyl groups have different ionization states in the complex formed with the asymmetric drug KNI-272. *Biochemistry 35*, 9945–9950.
38. Case, D. A., et al. (2006)Amber 9.0, University of California, San Francisco, CA.
39. Wang, J., Wang, W., Kollman, P. A., and Case, D. A. (2006) Automatic atom type and bond type perception in molecular mechanical calculations. *J. Mol. Graphics Model. 25*, 247–260.
40. Senapati, S., Cheng, Y., and McCammon, J. A. (2006) In-situ synthesis of a tacrine-triazole-based inhibitor of acetylcholinesterase: Configurational selection imposed by steric interactions. *J. Med. Chem. 49*, 6222–6230.
41. Yang, L., Beard, W. A., Wilson, S. H., Roux, B., Broyde, S., and Schlick, T. (2002) Local deformations revealed by dynamics simulations of DNA polymerase β with DNA mismatches at the primer terminus. *J. Mol. Biol. 321*, 459–478.
42. Duan, L. L., Tong, Y., Mei, Y., Zhang, Q. J., and Jhang, J. Z. H. (2007) Quantum study of HIV-1 protease bridge water interaction. *J. Chem. Phys. 127*, 145101–14506.
43. Chaitanya, V. S. V., and Senapati, S. (2008) Self-assembled reverse micelles in supercritical CO_2 entrap protein in native state. *J. Am. Chem. Soc. 130*, 1866–1870.

BI8006725